SPE 166512

Joint Inversion of Production and Temperature Data for Identification of Permeability Distribution with Depth in Deep Reservoirs

Zhishuai Zhang, University of California, Berkeley; Behnam Jafarpour, University of Southern California

This paper was prepared for presentation at the SPE Annual Technical Conference and Exhibition held in New Orleans, Louisiana, USA, 30 September–2 October 2013.

Abstract

Characterization of permeblity variation with depth in compartmentalized deep aquifers, geothermal and hydrocarbon reservoirs is important for prediction of flow and transport in complex subsurface environments and directly affects the development of natural and energy resources. In deep formations, temperature gradient can be significant and temperature data can provide valuable information about fluid displacement and conductivity in the vertical extent of the formation. This paper examines the importance of temperature data in resolving permeability distribution with depth by integrating flow and temperature data jointly and individually. We show that incorporation of temperature data in model calibration of deep aquifers can increase the resolution of permeability distribution profile with depth. To illustrate the importance of temperature measurements, we adopt a coupled heat and fluid flow model as a forward model to predict the heat and fluid transport in an a deep reservoir and perform a series of numerical experiments for integration of flow data alone, temperature data alone, and flow and temperature data jointly. For model calibration, we use the Maximum A-Posteriori (MAP) estimation approach and for uncertainty quantification we apply the Randomized Maximum Likelihood (RML). We develop an adjoint model for the coupled fluid and heat flow system of equations to compute the required gradients for model calibration. Investigation of the sensitivity of temperature and production data to the distribution of permeability shows that while fluid flow rate data can primarily resolve the distribution of permeability in the lateral extent of the reservoir, the fluid temperature data, even when measured at the surface, show sensitivity to permeability variability with depth, allowing for a higher resolution profiling of the permeability map. The results elucidate the value of temperature data in enhancing the resolution of the estimated aquifer permeability maps with depth.

Introduction

Numerical simulation of flow and transport processes in porous media is widely used to predict the fluid flow behavior in complex geologic formations. Accurate predictions hinges on reliable knowledge of rock hydraulic properties such as permeability. Since direct measurement of rock hydraulic properties is often not feasible, these properties are usually estimated from interpolation of scattered static data and low resolution seismic maps. Incorporation of aquifer dynamic response into prior aquifer model is often carried out through inverse modeling. In model calibration, it is common to use well flow rate and head measurements to estimate reservoir properties. However, the limitation in available observations complicates the estimation of reservoir properties, especially when heterogeneity is taken into account. In deep hydrocarbon and geothermal reservoirs, temperature variations with depth can be quite significant (*Hutchinson et al*. 2007; *Arnold et al*. 2010). Due to this temperature gradient, the fluids produced from different layers of the reservoir have different temperatures (higher temperatures with depth). Thus, the flowing fluid temperature is expected to carry information about flow-related property distributions with depth. In addition, modern monitoring technologies such as distributed permanent down-hole gauges (down-hole fiber optic temperature sensors) offer relatively inexpensive continuous measurements of pressure and temperature at various depths in the borehole (*Fryer et al.*, 2005; *Nath et al.*, 2006). Fiber optic sensors are used in both oil and gas reservoirs and geothermal reservoirs (Kragas, Williams et al. 2001; IKEDA

Naotsugu 2002). Continuous measurements of the down-hole pressure and temperature provide important monitoring data for real-time characterization and development plans.

To integrate temperature and fluid flow measurements into aquifer/reservoir models, coupled subsurface flow and heat transport must be used as forward model. Commercial software can be used for numerical simulation of coupled fluid flow and heat transport in porous media (e.g., *Pruess et al*. 1999). In addition, calibration of non-isothermal reservoir models from various observations has been investigated using several methods, including Maximum A Posteriori (MAP) estimation, Markov Chain Monte-Carlo (MCMC) approach, and the ensemble Kalman filter (EnKF) (*Woodbury and Smith*, 1988; *Rath et al*. 2006; *Kiryukhin et al*., 2008; *Kühn and Gessner*, 2009; *Mukhopadhyay*, 2009; *Vogt et al*. 2012). Very few of these studies consider the heterogeneity of reservoir properties. Bayesian inversion theory is commonly applied to parameter estimation problems, where the goal is to characterize the posterior probability density function (PDF) of the uncertain parameters by combining their prior PDF with the observed data, through a likelihood function (*Tarantola*, 2005; *Oliver et al*. 2008). Complete characterization of the posterior PDF is only possible under very limiting assumptions (e.g., linear Gaussian case) that are not met in real applications where large-scale nonlinear flow and transport models are used. In such cases, probabilistic inversion methods aim to either estimate point statistics (e.g., mean, variance) of the parameter posterior PDF, e.g., the MAP estimate, or approximate the posterior PDF by generating several realizations from it, e.g., RML, EnKF and MCMC methods, (*Kitanidis*, 1995; *Evensen*, 1994; *Oliver et al*. 1996; *Tarantola*, 2005; *Oliver et al*. 2008, *Vrugt et al*., 2008, *Henricks Franssen et al.*, 2009). A main advantage of the latter approach is that it provides a practical framework for uncertainty quantification.

In this paper, we consider the MAP estimation approach for joint inversion of flow and temperature data and apply the RML method for uncertainty quantification. The MAP and RML estimation approaches involve the solution of an optimization problem. Gradient-based solution methods can be used to obtain these estimates. They are efficient when the gradient of the optimization objective function with respect to the unknown parameters is readily available, e.g. through the adjoint method (*Neuman and Carrera*, 1985; *Giering and Kaminski*, 1998; *Oliver et al*. 2008). In this paper, we implement the adjoint method for coupled fluid flow and heat transport to compute the gradients required for joint inversion of flow and temperature observations. The remainder of this paper is organized as follows. We first present the principles and modeling approach for coupled simulation of fluid and heat flow and the adjoint method for gradient calculation, followed by a brief overview of the MAP and RML estimation methods. We then present the experimental setup and show the results of applying the MAP and RML methods to characterization of heterogeneous reservoirs, before presenting the conclusions.

Coupled Fluid and Heat Flow Equations

To implement the joint inversion of flow rate and temperature data, a coupled fluid and heat flow model is needed (as a forward model) to relate the observations of produced fluid flow rates and temperatures to uncertain input model parameters. Here we first present the underlying equations of our forward model, followed by the general Bayesian inversion framework.

Non-isothermal Flow Model

Coupled fluid and heat flow in porous media has been studied for many years, and a comprehensive approach is presented in (*Bejan*, 2004). The governing equations are derived from a combination of mass conservation and energy conservation equations with Darcy's law.

Non-isothermal Flow Model

Coupled fluid and heat flow in porous media has been studied for many years, and a comprehensive approach is presented in (*Bejan*, 2004). The governing equations are derived from a combination of mass conservation and energy conservation equations with Darcy's law. After combining the energy equations for solid and fluid parts and incorporating Darcy's Law, the final equation describing the fluid flow and heat transport can be expressed as

$$\rho_f c_{pf}\left(\sigma\frac{\partial T}{\partial t}+\vec{v}\cdot\nabla T\right)=\nabla\cdot(k\nabla T)+\rho_{f0}\tilde{q}c_{pf}(T_s-T)+\beta_f T\Phi\frac{\partial P}{\partial t}+\beta_f T\vec{v}\cdot\nabla P+\frac{\mu}{K}(\vec{v})^2 \quad (1)$$

where the notations used are as follows:
$\rho =$ density of fluid in reservoir condition
$\rho_0 =$ density of fluid at standard condition
$\vec{v} = u\hat{\imath} + v\hat{\jmath} + w\hat{k} =$ velocity of fluid,

$\tilde{q}$ = volume of injected (+) or produced (-) fluid at standard condition in unit reservoir volume and unit time
$\frac{D}{Dt} = \frac{\partial}{\partial t} + u\frac{\partial}{x} + v\frac{\partial}{y} + w\frac{\partial}{z}$ = material derivative
P = fluid pressure
k = fluid thermal conductivity
μ = fluid viscosity
$\mu\Phi$ = viscous dissipation term
Φ = a function of the spatial derivative of velocity (in two dimension $\Phi = 2\left[\left(\frac{\partial u}{\partial x}\right)^2 + \left(\frac{\partial u}{\partial y}\right)^2\right] + \left(\frac{\partial u}{\partial y} + \frac{\partial v}{\partial x}\right)^2$)
T_s = temperatures of the fluid going into the system
T = temperatures of the fluid going out of the system
c_p = constant pressure heat capacity of the liquid
β = coefficient of thermal expansion (for an incompressible fluid $\beta = 0$ and for an ideal gas $\beta T = 1$)
$\sigma = \frac{\Phi\rho_f c_{pf} + (1-\Phi\rho_s c_{ps})}{\rho_f c_{pf}}$.

In this paper, we use a finite difference numerical scheme to solve the above coupled fluid and heat flow equations to predict the evolution of fluid flow and temperature in an aquifer. The time evolution of these state variables can predict the flowing rate and temperature at each well as a function of input model parameters (e.g., aquifer permeability distribution). In the next section, we present the general Bayesian inverse modeling framework for conditioning uncertain aquifer permeability distributions on observed flow rate and temperature measurements. We apply this framework for joint inversion of flow rate and temperature data to study the role of fluid flow temperature on constraining the permeability in the vertical extent of aquifers.

Bayesian Inverse Modeling Approach

In this section we present a brief overview of the MAP and RML estimation methods. We assume a Gaussian prior PDF for the parameters $\mathbf{m}$ and a Gaussian likelihood model to represent the measurements $\mathbf{d_{obs}}$. We consider the measurement model $\mathbf{g(m)}$ as a nonlinear function of the parameters. The conditional PDF of the unknown parameters can be expressed by invoking the Baye's rule (*Tarantola*, 2005)

$$f(\mathbf{m}|\mathbf{d_{obs}}) = f(\mathbf{d_{obs}}|\mathbf{m})f(\mathbf{m})/f(\mathbf{d_{obs}}) \tag{2}$$

Assuming a Gaussian prior PDF

$$f(\mathbf{m}) = c_1 \exp\left[-\frac{1}{2}\left(\mathbf{m}-\mathbf{m_{prior}}\right)^T \mathbf{C_m^{-1}}\left(\mathbf{m}-\mathbf{m}_{prior}\right)\right] \tag{3}$$

and likelihood function

$$f(\mathbf{d_{obs}}|\mathbf{m}) = c_2 \exp\left[-\frac{1}{2}(\mathbf{g(m)}-\mathbf{d_{obs}})^T \mathbf{C_d^{-1}}(\mathbf{g(m)}-\mathbf{d_{obs}})\right] \tag{4}$$

and using simple algebraic manipulations, the posterior PDF can be reduced to (Tarantola, 2005)

$$f(\mathbf{m}|\mathbf{d_{obs}}) = a \exp\left[-\frac{1}{2}\left(\mathbf{m}-\mathbf{m_{prior}}\right)^T \mathbf{C_m^{-1}}\left(\mathbf{m}-\mathbf{m}_{prior}\right) - \frac{1}{2}(\mathbf{g(m)}-\mathbf{d_{obs}})^T \mathbf{C_d^{-1}}(\mathbf{g(m)}-\mathbf{d_{obs}})\right] \tag{5}$$

where a is a normalizing constant. In the above equations, $\mathbf{m}$ is a $N_m$dimensional column vector with prior mean and covariance $\mathbf{m_{prior}}$ and covariance $\mathbf{C_m}$, respectively, and $\mathbf{d} = \mathbf{g(m)}$ is a N_d dimensional vector containing the observable quantities with mean $\mathbf{d_{obs}}$ and covariance $\mathbf{C_d}$. For the nonlinear measurement operator $\mathbf{d} = \mathbf{g(m)}$, the posterior PDF in Eq. (4) takes a more complex non-Gaussian form that, in general, cannot be represented analytically. Two general approaches are considered in the literature for characterization of the resulting posterior PDF. The first approach aims to estimate important point statistics of the posterior PDF, such as its mean and covariance, which provide incomplete, yet important, characterization of the conditional parameter distribution. The second class of methods focuses on approximating the posterior PDF by generating several conditional realizations (e.g., MCMC and RML), that enable a systematic approach uncertainty quantification for the flow and transport predictions. We adopt the MAP and RML estimation methods and focus our attention on evaluating the importance of temperature data in enhancing the estimation of reservoir permeability distribution with depth.

Maximum A Posteriori Estimate

The MAP estimate $\mathbf{m}_{MAP}$ is the model that maximizes the conditional PDF $f(\mathbf{m}|\mathbf{d_{obs}})$

$$\mathbf{m_{MAP}} = \text{argmin}_m\, O(\mathbf{m}) \tag{6}$$

or equivalently minimizes (using Gaussian assumptions)

$$O(\mathbf{m}) = \frac{1}{2}\left(\mathbf{m}-\mathbf{m_{prior}}\right)^T \mathbf{C_m^{-1}}\left(\mathbf{m}-\mathbf{m_{prior}}\right) + \frac{1}{2}(\mathbf{g(m)}-\mathbf{d_{obs}})^T \mathbf{C_d^{-1}}(\mathbf{g(m)}-\mathbf{d_{obs}}) \tag{7}$$

The above minimization can be implemented using the classical Newton approach. By taking the derivative of the objective function in Eq. (6) with respect to $\mathbf{m}$ and rearranging, we get the following iterations that at convergence yields a local solution

$$\mathbf{m}^{n+1} = \left[\left(\mathbf{C_m^{-1}} + \mathbf{C_m^{-1}}^T\right) + \mathbf{G}^{nT}\left(\mathbf{C_d^{-1}} + \mathbf{C_d^{-1}}^T\right)\mathbf{G}^n\right]^{-1}$$
$$\left[\left(\mathbf{C_m^{-1}} + \mathbf{C_m^{-1}}^T\right)\mathbf{m_{prior}} + \mathbf{G}^{nT}\left(\mathbf{C_d^{-1}} + \mathbf{C_d^{-1}}^T\right)(\mathbf{d_{obs}} - \mathbf{g}(\mathbf{m}^n) + G^n\mathbf{m}^n)\right] \tag{8}$$

Here, $\mathbf{G}$ is the sensitivity matrix with elements $G_{ij} = \frac{\partial g_i}{\partial m_j}$. Once the MAP estimate $\mathbf{m}_{MAP}$ is found, the posterior covariance matrix $\mathbf{C}_{\mathbf{m},MAP}$ can be approximated through linearization about the MAP estimate as

$$\mathbf{C}_{\mathbf{m},MAP} = \left(\mathbf{G}_{MAP}^T \mathbf{C_d^{-1}} \mathbf{G}_{MAP} + \mathbf{C_m^{-1}}\right)^{-1} \tag{9}$$

The gradients required for carrying out the the iteration in Eq. (8) can be efficiently computed using the adjoint method (Oliver et al., 2008).

Randomized Maximum Likelihood

A practical approach for uncertainty assessment is to generate multiple realizations of the conditional PDF of the parameters. Theoretically rigorous sampling methods such as MCMC can be applied to generate conditional realizations. However, these methods are computational too demanding for practical applications where large-scale nonlinear flow and transport models are considered (*Liu and Oliver*, 2003). The RML is proposed as an approximate method for sampling from the posterior PDF (*Kitanidis*, 1995; *Oliver*, 1996). When the data and model are related linearly, the RML can be shown to correctly sample the posterior PDF (*Oliver* 1996). For nonlinear data and model relation that are frequently encountered in practice, the method is considered a an approximate conditional sampling technique. Computational results indicate that even for weakly nonlinear problems, such as single-phase flow the RML sampling provides a reasonable characterization of the posterior PDF (*Oliver*, 1996; 1999; *Liu and Oliver* 2003). The RML formulation for conditioning an unconditional realization on flow data leads to minimizing the objective function

$$S(\mathbf{m}) = \left(\mathbf{m}-\mathbf{m}_{u,i}\right)^T \mathbf{C_m^{-1}}\left(\mathbf{m}-\mathbf{m}_{u,i}\right) + \left(\mathbf{g(m)}-\mathbf{d}_{u,i}\right)^T \mathbf{C_d^{-1}}\left(\mathbf{g(m)}-\mathbf{d}_{u,i}\right) \tag{10}$$

where $\mathbf{m}_{u,i}$ is an unconditional realization of the model variable, $\mathbf{d}_{u,i}$ represents an instance of the data vector with a Gaussian noise distribution, $\mathbf{m}_{c,i}$ denotes the conditional realization that minimizes the objective function in Eq. (10). To generate *N* conditional realizations using the RML approach, the above optimization must be solve *N* time each starting with a different instances of the unconditional parameters $\mathbf{m}_{u,i}$ and measurements $\mathbf{d}_{u,i}$.

Experiment Setup

We consider a non-isothermal three-dimensional single phase flow system in a geothermal reservoir. The information about the reservoir model and simulation parameters can be found in Tables 1 through 3. Table 4 contains the parameter used for geostatistical simulation of the reference model and the unconditional realizations used for the RML implementation. The initial temperature on the top layer of the reservoir is 100 °C and that on the bottom layer is 200 °C. The geothermal gradient is assumed to be constant within the reservoir. The configuration of the reservoir model and the initial temperature distribution are given in Fig. 1a. Water at room temperature (20 °C) is injected through the injection well in the middle of the reservoir and is produced from the eight production wells symmetrically located on the edges of the domain. The observations of pressure at injection well and flow rate and temperature at the production wells are used for estimation of the permeability map. The observations were generated by running the forward simulation with a reference permeability model and adding 2% uncorrelated observation error to the simulation results.

To model distributed temperature measurements, in some experiments we also included temperature data from each layer of the formation at each production well. The injection well is rate controlled while each of the

production wells operates with a constant pressure of 2900 psi (initial field pressure is 3000 psi). Fluid production rate at each well is measured as the sum of the production rate from different layers. The observed production temperature is the flow rate weighted mean of the production temperature at each production layer. We also consider a case with permanent downhoe sensors deployed to measure the produced fluid temperature at each layer (*Kragas et al.*, 2001). The well index of the production well is obtained from Peaceman's model (Peaceman, 1978). The liquid properties of water were used in these experiments. The logarithm of true permeability map and the true heat conductivity map are generated by drawing two samples from the sequential Gaussian simulation based on the variogram parameters reported in Table 4. The Stanford Geostatistical Modeling Software SGSIM was used to generate the true and prior realizations in this study, all using the same variogram model (*Remy et al*. 2008).

Results and discussion

MAP Estimation Results

Figure 1 summarizes the field setup and reference models. The field configuration and well locations as well as the true heat conductivity and log-permeability maps and the uniform permeability as an initial model for this experiment are shown in Figs. 1a through 1d, respectively. The permeability characterization results with different measurement types are presented in Fig. 2. The permeability map estimated from only the production rate (first column) shows homogeneity along the vertical direction. However, when conditioned on production temperature (the second and third columns), the conditional permeability indicates heterogeneity along the vertical direction that is consistent with the reference permeability model. This shows that the fluid temperature data is capable of resolving the vertical distribution of aquifer permeability. When measured at the surface, the flow data mainly conveys information about the horizontal distribution of the aquifer permeability and does not provide much vertical resolution. The temperature data, on the other hand, shows sensitivity to the permeability in each aquifer layer since geothermal gradient results in lower temperatures on the upper layers of the aquifer. As a result, if the permeability on the upper layer is higher, the produced fluid will have a lower temperature. Consequently, observations of production temperature can reveal information about the contribution of each aquifer layer to the produced water. The sensitivity analysis, shown on the last two rows of Fig. 2, further demonstrates this point. From these plots, we observe that the sensitivity maps of the production rate have the same sign along the vertical direction while those for the production temperature have opposite signs. Hence, conditioning the permeability estimation on both production rate and temperature improves the resolution of the permeability map in the vertical direction. The performance of each method is quantified using a root-mean-squared error measure that is summarized in Table 4. These results show that the estimation quality increases with addition of a new data type, which is an expected outcome.

To further study the effect of temperature data measured by downhole fiber optic sensors, we integrated temperature data from distributed permanent downhole sensors at each layer of the formation in the production wells. The estimation results for this case are shown in the fourth column of Fig. 2. The MAP estimate of the permeability distribution shows a higher resolution than those obtained without downhole temperature sensors. This is because the distributed temperature data provide more detailed information about the "average" permeability in each layer by measuring the cold water breakthrough at each layer. In the absence of distributed temperature sensors, the permeability of each layer has to be inferred from the temperature of the mixed fluid from all layers measured at the surface. The estimated variance maps also convey important information about the information content in each data type. When only flow rate data is integrated, a significant portion of the variance, especially in the vertical direction, remains in the solution. As the information content of the data in the vertical direction increases (by adding temperature data) so does the resolution of the estimated maps. Similar conclusions can be drawn by examining the sensitivity maps on the last two rows of Fig. 2.

While the permeability MAP and variance estimates provide important information about the likely distribution of permeability and its corresponding confidence, respectively, they do not provide a systematic approach for estimating the flow prediction uncertainties. A practical approach to uncertainty quantification is achieved through Monte-Carlo simulation and ensemble forecasting. Markov Chain Monte-Carlo (MCMC) methods provide a rigorous approach for sampling from the posterior distribution (Tarantola, 2005). However, they suffer from prohibitive computational costs that limit their practical applications. In the next section, we present the randomized maximum likelihood (RML) as an approximate sampling that for linear-Gaussian models reduces to exact sampling from the poster distribution and has been shown to provide reasonable results for mildly nonlinear models, without any formal convergence proof.

RML for Uncertainty Quantification

While the MAP estimation results give important information about the overall distribution of the permeability in the field, it cannot be used to generate multiple realizations of the permeability field that are conditioned on the dynamic data. Here, we present the results from applying the RML approach to generate multiple conditional models that can be used for uncertainty quantification and risk assessment. We first generate N=100 unconditional log-permeability realizations $\mathbf{m}_{u,i}$ using the prior variogram/covariance model and the same number of measurement instances $\mathbf{d}_{u,i}$ based on the data noise distribution model. The parameters used for geostatistical simulation of the prior realizations are reported in Table 4. Each pair of the resulting realizations $(\mathbf{m}_{u,i}, \mathbf{d}_{u,i})$ is then used in forming the RML objective function in Eq. (10), which is minimized using a gradient-based algorithm. The gradients are efficiently calculated by an adjoint model.

The RML estimation results are summarized in Figs. 3 and 4. Figure 3a contains the sample mean (left) and standard deviation (right) maps for the unconditional realizations. In Fig. 3b, the same results are shown after conditioning on rate, surface and sensor temperature data. On average, similar to the MAP estimates, the RML results also identify the main high and low permeability trends in the field. Figures 4a and 4b display six randomly selected unconditional and conditional realizations, respectively. The conditioning data include production flow rate and temperature, as well as the temperature measured at each layer by the distributed sensors in the wells. It is evident from these plots that the permeability realizations exhibit more detailed heterogeneity than the MAP estimate. Each of the calibrated realizations captures the overall field connectivity and permeability trend. However, given the local nature of the gradient-based optimization used it is possible that some of the realization may have been trapped in a local solution. In such cases, the solution can be discarded if the resulting data match (likelihood function) becomes unacceptable. We did not observe large mismatches in our experiments.

Conclusion

We studied the role of temperature data in the estimation of permeability in geologic formations that exhibit thermal gradient. We developed a coupled heat and fluid flow model by taking into account advection, thermal conduction, thermal expansion, and viscosity dissipation effects and used the finite difference method to numerically solve these equations to predict fluid and heat flow response of the formation under a given heat production scenario. We also derived the numerical adjoint model for the coupled heat and fluid flow equations to efficiently compute the gradients of the well response quantities with respect to aquifer permeability. We evaluated the effect of temperature data on estimating the permeability distribution using two estimation methods: the MAP approach and the RML method. While the MAP estimate provides the most likely estimate of the posterior distribution, the RML estimation method provides multiple conditional realizations of the permeability map that can be useful for uncertainty quantification. These methods were used to integrate, individually and in combination, three different data types, i.e. water production rate, water production temperature at the surface and measured temperature at each layer from distributed sensors that are deployed in the well. The estimation results suggest that while the production rate data convey information on permeability heterogeneity mainly along the horizontal direction, production temperature, even when it is only measured at the surface, reveals complementary permeability information along the vertical direction. This is attributed to the temperature data content, which in this case combines the information about the vertical temperature gradient in the formation with the flow contribution from each layer. Since the flow contribution at each layer is governed by the respective permeability in that layer, temperature measurements contain information about permeability distribution at different layers, which can be integrated to enhance the permeability distribution in the vertical extent of the formation. Temperature data can play a significant role in characterization of deep aquifers, dipped reservoirs, and geothermal resources that exhibit significant temperature variations.

References

Arnold G., Cavalero S.R., Clifford P.J.; Goebel E.M., Hutchinson D.A., Leung E.N., Weiss T.D., Grass D.B. (2010): Thunder Horse and Atlantis Deepwater Frontier Developments in the Gulf of Mexico: Thunder Horse Takes Reservoir Management to the Next Level. Paper OTC 20396 MS presented at the Offshore Technology Conference, Houston, Texas, 3-6 May. DOI: 10.4043/20396-MS.

Bejan A. (2004): *Convection Heat Transfer*. New York City: John Wiley & Sons.

Evensen, G. (1994), Sequential data assimilation with a non-linear quasigeostrophic model using Monte Carlo methods to forecast error statistics, *J. Geophys. Res., 99*(C5), 10,143–10,162.

Finsterle S. (1999): *Itough2 User's Guide*, Berkeley, CA: Lawrence Berkeley National Laboratory.

Franssen, H. H., Alcolea, A., Riva, M., Bakr, M., van de Wiel, N., Stauffer, F., and Guadagnini, A. (2009), A comparison of seven methods for the inverse modelling ofgroundwater flow. application to the characterisation of well catchments, *Advances in Water Resources*, 32(6), pp. 851-872 doi:10.1016//j.advwatres.2009.02.011.

Fryer V.I., Dong S., Otsubo Y. et al. (2005): Monitoring of Real-Time Temperature Profiles across Multizone Reservoirs During Production and Shut in Periods Using Permanent Fiber-Optic Distributed Temperature Systems. Paper SPE 92962 MS presented at the SPE Asia Pacific Oil and Gas Conference and Exhibition, Jakarta, Indonesia, 5-7 April. DOI: 10.2118/92962-MS.

Giering R., Kaminski T. (1998): Recipes for Adjoint Code Construction. *ACM Transactions on Mathematical Software (TOMS)* **24** (4): 437-474. DOI: 10.1145/293686.293695.

Hutchinson D., Kuramshina N., Sheydayev A. (2007). The New Interference Test: Reservoir Connectivity Information from Downhole Temperature Data. Paper SPE 11672 MS presented at International Petroleum Technology Conference, Dubai, U.A.E., 4-6 December. DOI: 10.2523/11672-MS.

Jafarpour B., McLaughlin D.B. (2009): Reservoir characterization with discrete cosine transform, part-1: parameterization, part-2: history matching. *Soc. Pet. Eng. Journal;*14(1): 182-201.

Jafarpour B., Tarrahi M. (2011): Assessing the performance of the ensemble Kalman filter for subsurface flow data integration under variogram uncertainty, Water Resources Research, 47, W05537, 26 PP.

Kiryukhin A.V., Asaulova N.P., Finsterle S. (2008): Inverse Modeling and Forecasting for the Exploitation of the Pauzhetsky Geothermal Field, Kamchatka, Russia. *Geothermics* **37** (5): 540-562.

Kitadinis P. (1995): Quasi-linear Geostatistical Theory for Inversing, *Water Resources Research,* 31(10), pp. 2411-2419.

Vogt C., Marquart G., Kosack C., Wolf A., Clauser A. (2012). Estimating the permeability distribution and its uncertainty at the EGS demonstration reservoir Soultz-sous-Forêts using the ensemble Kalman filter,Water Resources Research, 48(8), DOI: 10.1029/2011WR011673.

Kragas T.K., Williams B.A., Myers G.A. (2001): The Optic Oil Field: Deployment and Application of Permanent in-Well Fiber Optic Sensing Systems for Production and Reservoir Monitoring. Paper SPE 71529 MS presented at the SPE Annual Technical Conference and Exhibition, New Orleans, Louisiana, 30 September-3 October. DOI: 10.2118/71529-MS.

Kühn M., Gessner K. (2009): Coupled Process Models of Fluid Flow and Heat Transfer in Hydrothermal Systems in Three Dimensions. *Surveys in geophysics* **30** (3): 193-210. DOI: 10.1007/s10712-009-9060-8.

Liu N., Oliver D. (2003): Evaluation of Monte Carlo Methods for Assessing Uncertainty. *SPE Journal* **8** (2): 188-195.

Marchuk G.I., Agoshkov V.I., Shutiaev V. (1996): *Adjoint Equations and Perturbation Algorithms in Nonlinear Problems*. Florence, KY: CRC.

Mukhopadhyay S. (2009): Parameter Estimation from Flowing Fluid Temperature Logging Data in Unsaturated Fractured Rock Using Multiphase Inverse Modeling. *Water Resour. Res.* **45** (4): W04414. DOI: 10.1029/2008wr006869

Nath D.K., Finley D.B., Kaura, J.D. (2006): Real-Time Fiber-Optic Distributed Temperature Sensing (DTS)-New Applications in the Oil Field. Paper SPE 103069 MS presented at the SPE Annual Technical Conference and Exhibition, San Antonio, Texas, 24-27 September. DOI: 10.2118/103069-MS.

Neuman S., Carrera J. (1985): Maximum-Likelihood Adjoint-State Finite-Element Estimation of Groundwater Parameters under Steady-and Nonsteady-State Conditions. *Applied mathematics and computation* **17** (4): 405-432. DOI: 10.1016/0096-3003(85)90043-8.

Oliver D.S., He N., Reynolds A.C. (1996): Conditioning Permeability Fields to Pressure Data. Paper presented at 5th European Conference on the Mathematics of Oil Recovery, Mining University Leoben, Austria, September 3-6.

Oliver D.S., Reynolds A.C., Liu N. (2008): *Inverse Theory for Petroleum Reservoir Characterization and History Matching*. Combridge, UK: Cambridge Univ Press.

Peaceman D.W. (1978): Interpretation of Well-Block Pressures in Numerical Reservoir Simulation. *Old SPE Journal* **18** (3): 183-194.

Pruess K., Oldenburg C., Moridis G. (1999). *Tough2 User's Guide*, Berkeley, CA: Lawrence Berkeley National Laboratory.

Rath V., Wolf A., Bücker H. (2006): Joint Three-Dimensional Inversion of Coupled Groundwater Flow and Heat

Transfer Based on Automatic Differentiation: Sensitivity Calculation, Verification, and Synthetic Examples. *Geophysical Journal International* **167** (1): 453-466. DOI: 10.1111/j.1365-246X.2006.03074.x.

Remy N., Boucher A., Wu J. (2008): *Applied Geostatistics with Sgems: A User's Guide. Combridge,* UK: Cambridge Univ Press.

Somerton W., Keese J., Chu S. (1973): Thermal Behavior of Unconsolidated Oil Sands. *Old SPE Journal* **14**(5): 513-521. DOI: 10.2118/4506-PA.

Tarantola A. (2005): *Inverse Problem Theory and Methods for Model Parameter Estimation*: Society for Industrial Mathematics.

Vrugt J.A., Ter Braak C.J.F., Clark M.P., Hyman J.M., Robinson B.A. (2001): Treatment of input uncertainty in hydrologic modeling: Doing hydrology backward with Markov chain Monte Carlo simulation, Water Resour. Res, 44(12), W00B09.

Woodbury A.D., Smith, L. (1988): Simultaneous inversion of hydrogeologic and thermal data: 2. Incorporation of thermal data, Water Resources Research, 24(3), pp. 356–372.

Tables

Table 1. General simulation parameters

Properties	*Value*
Simulation time	1000 days
Observation interval	50 day
Reservoir Dimension	$1260.0 \times 1260.0 \times 660.0$
Grid system	$21 \times 21 \times 11$
Cell dimension	$60.0 \times 60.0 \times 60.0$ feet
Initial pressure	2920 psi
Boundary conditions	No flow boundary conditions
Production rate error	2 %
Production temperature error	2 %
Injection pressure error	2 %
Temeprature sensor error	2 %
Gravity	$0\ m/s^2$ (Neglected)

Table 2. Field configuration

Properties	*Value*
Number of injectors	8
Number of producers	1
Well index Model	Peaceman's model(Peaceman 1978)
Total injection rate	66000 BBL/Day
Injection fluid temperature	20 °C
Production well radius	0.583 feet
Production well BHP	2900 psi
Observation at the injection well	Pressure
Observation at production wells	Surface flow rate and temperature
Observation at deployed sensors	Well flow temperature (each layer)

Table 3. Rock and fluid properties

Properties	*Value*
Rock porosity	0.2
Rock heat capacity	0.84×10^3 J/K
Rock density	2.7×10^3 kg/m^3
Fluid reference density	1×10^3 kg/m^3
Fluid heat capacity	4.19×10^3 J/K
Fluid compressibility	3×10^{-6} (1/psi)
Fluid thermal expansion coefficient	207 (10^{-6}/°C)
Pressure at fluid reference density	2800 psi
Temperature at fluid reference density	20 °C
Fluid viscosity model	Likhachev's model (2003)

Table 4. Geostatistical simulation parameters

Properties	*Value*
Kriging type	Ordinary Kriging
Max conditioning data	12
Search Ellipsoid Ranges	21×21×6
Search Ellipsoid Angles	0×0×0
Variogram model	Spherical
Nugget Effect	0
Logarithm permeability contribution (Sill)	1 $\ln^2(mD)$
Thermal conductivity contribution (Sill)	0.09 $W^2/(m \cdot K)^2$
Logarithm permeability mean	1 $\ln(mD)$
Thermal conductivity mean	3 $W/(m \cdot K)$

Table 5. Performance of MAP permeability estimation

	Rate	*Temp*	*Rate and Temp*	*Rate Temp Sensor*
RMSE	3.4341e+003	2.1451e+003	1.9020e+003	1.7837e+003

Figures

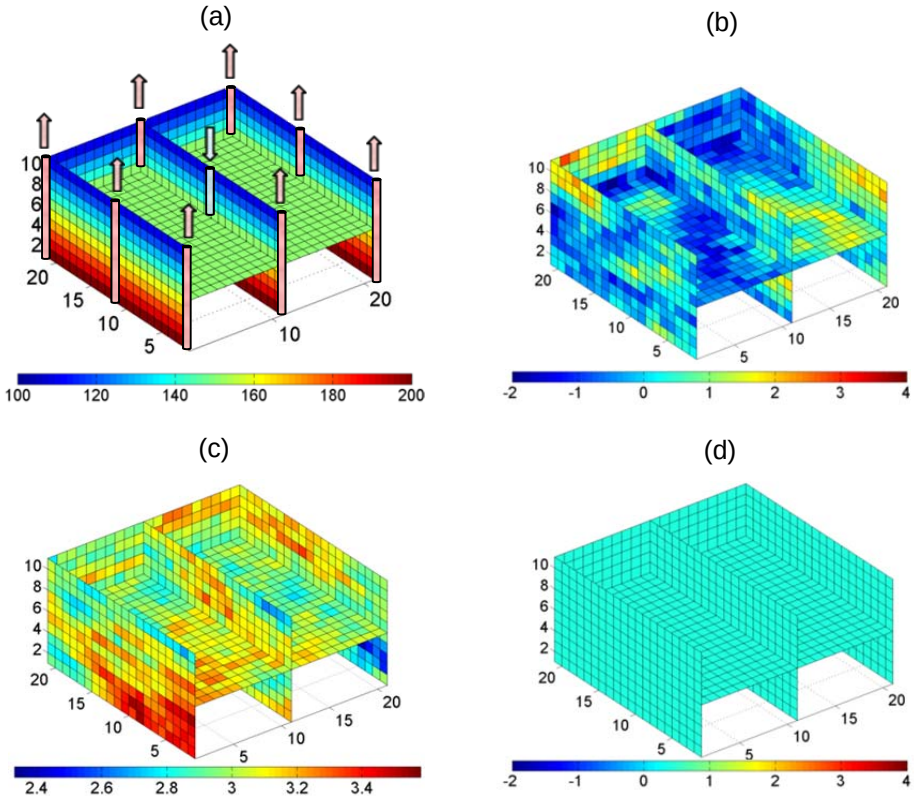

Fig. 1. (a) Field configuration and temperature gradient; (b) heterogeneous aquifer permeability distribution; (c) aquifer thermal conductivity distribution; (d) initial permeability field for the MAP estimation.

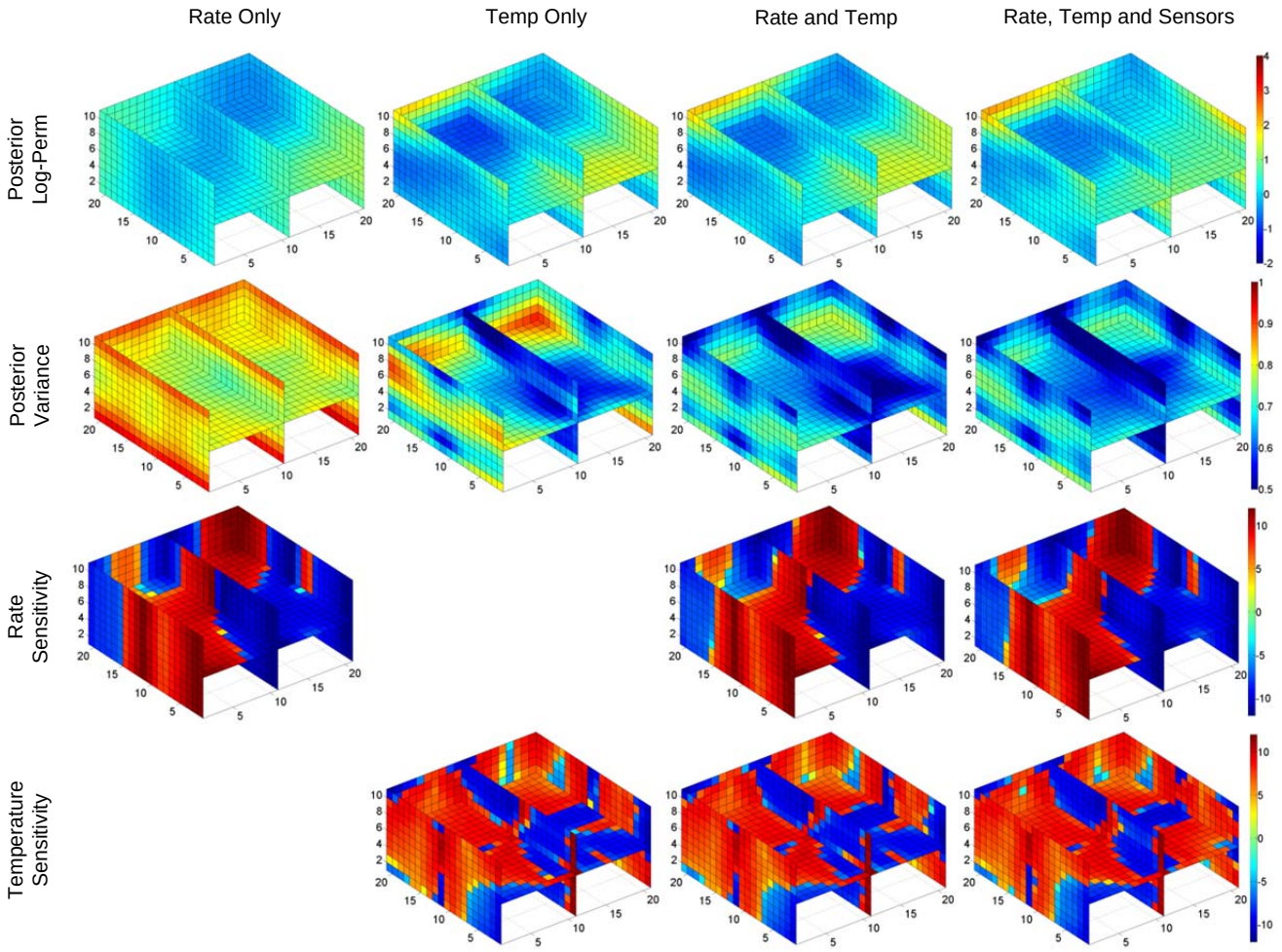

Fig. 2. MAP estimation result for different observations (columns); the MAP estimates and their corresponding variance maps are shown in rows one and two; rows three and four display the averaged flow rate and temperature observation sensitivities to the unknown permeability distribution, respectively; the estimation results are shown for flow rate only (first column), surface temperature only (second column), flow rate and surface temperature (third column), and flow rat, fluid temperature measured at the surface and fluid temperature measured at each layer by distributed sensors in the wells (fourth column).

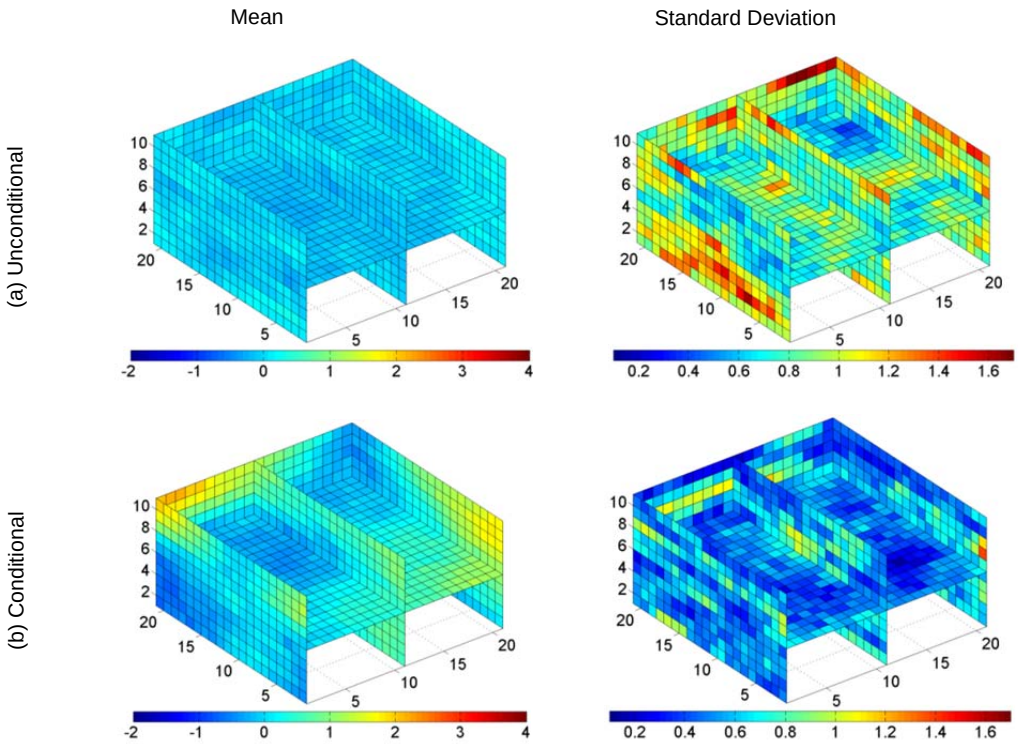

Fig. 3. The ensemble calculated estimation results for the RML approach; the ensemble mean (left) and variance (right) maps are shown for the unconditional (a) and conditional realizations. The conditional results are shown after integration all data types.

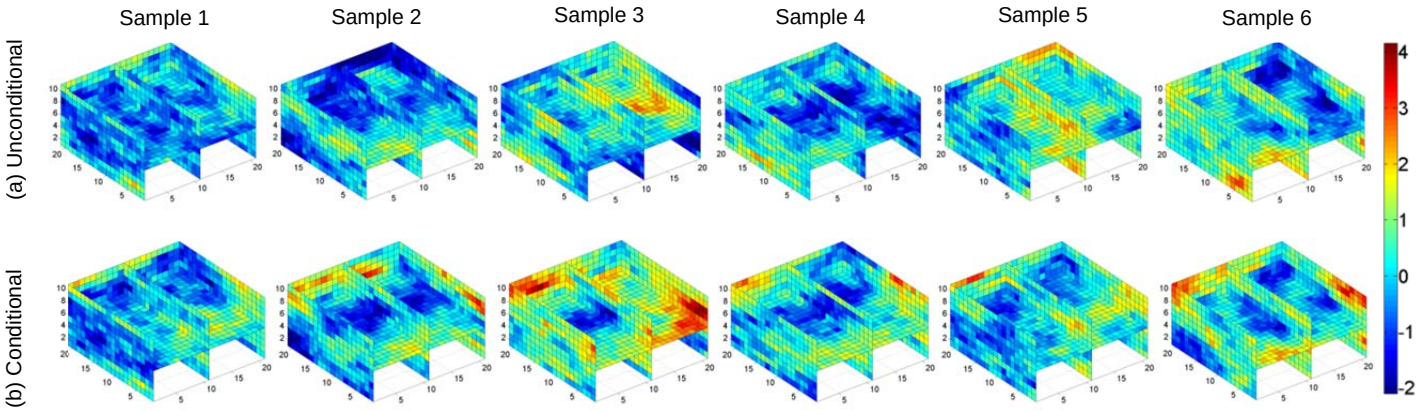

Fig. 4. Sample unconditional (a) and conditional (b) realizations of the permeability field from the RMLS estimation approach. The estimated permeability realizations tend to preserve the heterogeneity of the reference model.